DAΦNE TECHNICAL NOTE

INFN - LNF, Accelerator Division

Frascati, May 13, 1992

Note: **I-9**

DAΦNE ACCUMULATOR UPDATE-3

M.R. Masullo, C. Milardi, M.A. Preger

1. THE NEW LATTICE

A new working point above the integer in both planes has been chosen for the DAΦNE accumulator, with the main purpose of avoiding the resistive wall instability [1]. The betatron wave numbers are $Q_x = 3.12$, $Q_y = 1.14$.

The new lattice shows some other differences with respect to the previous one [2,3]: the quadrupoles have now the same magnetic length as in the DAΦNE main ring (30 cm), their position has been changed slightly in order to decrease the vertical β function in the kicker region and the sextupole positions have been moved to improve the dynamic aperture on the new working point, keeping at the same time the kicker strength at a reasonable level.

Table I is a MAD output for the linear lattice, while Table II shows the corresponding parameter list. The optical functions for 1/4 of the ring are plotted in Fig. 1. The machine layout is shown in Fig. 2. The magnetic strengths for the nominal working point are summarized in Table III.

The lattice upgrade improves injection acceptance as shown in Fig. 3, where the starting horizontal coordinates (x,x' phase space) of the particles coming from the Linac, going through the injection kickers and tracked through 100 turns are plotted; vertical and energy distributions have not been taken into account. On the same figure an ellipse is superimposed: the ellipse area is the Linac beam emittance (10 mm·mrad), while its shape ($\alpha = 0$, $\beta = 1.6$ m) provides the best matching to the accumulator acceptance. It can be pointed out that the beam from the Linac easily fits inside the accumulator acceptance and the optimum horizontal angle for injection has been reduced to -1.5 mrad.

In order to correct the chromaticity two sextupole families have been used (see Table III). Fig. 5 shows the dynamic aperture given by the tracking simulation code PATRICIA in the center of the injection straight section for particles with the nominal energy and with $\Delta E/E = \pm 1.5\%$, the result being similar to the previous one [3]. The dashed area (34 x 28 mm^2) corresponds to the physical aperture of the ring (limited by the injection and extraction septa in the horizontal plane and by the bending magnet gap in the vertical) scaled to the symmetry point with the square root of the betatron functions.

2. INJECTION AND EXTRACTION

The injection kicker intensity has been calculated in the approximation of localized angular perturbations. The injection philosophy requires vanishing residual oscillation of the stored beam and a stay clear distance for the bucket center of 4σ from the inner septum side. Calculations have been performed assuming a septum distance of 20 mm from the design orbit. Kicker intensities have been evaluated both for sextupoles on and off, with positrons injected in the clockwise direction and electrons in the opposite one (Table IV).

Extraction kickers must provide a nominal displacement d=-28 mm, for the bucket center, if the damped beam has to satisfy 3σ stay clear requirements at the extraction septum. Their number should be limited, as strongly recommended by the Machine Review Committee, in order to decrease the vacuum chamber impedance. In addition, to make the design of the pulsed power supply easier, it has been decided to avoid injection/extraction schemes where the polarity of the field changes during machine operation.

As a consequence beam extraction with three out of the four injection kickers (see Fig. 2) has been analyzed. The solutions are plotted in Fig. 6 for three different bucket center displacements at the extraction septum, each one as a function of the extraction angle. It is worth noticing that the required kicker strength shows a minimum near the optimum injection angle, which makes the design of the transport lines easier than in the previous scheme [3]. Moreover, the beam can be extracted, in most cases, by firing K1 and K2 only, K3 being of some help only when the extraction angle is smaller than the optimum one (remember that the sign of the angle changes between injection and extraction on the same trajectory). The required integrated field for the nominal extraction trajectory is $\approx$120 G·m. The same figures show (dotted lines) the kicker strengths with sextupoles off, which are slightly larger than those with the chromaticity correction, demonstrating that the chosen sextupole configuration is favourable for injection and extraction.

For sake of completeness, the possibility of using both field polarities at extraction in the kickers has been also studied. The results are given in Table V, showing that this option could decrease the required integrated fields by almost a factor two. Fig. 7 shows the injection and extraction trajectories with only positive polarity, Fig. 8 is the corresponding one when both polarities are used.

The injection efficiency has been estimated by means of a tracking code, starting from the septum with a uniform random horizontal distribution whose coordinates are within the phase space ellipse shown in Fig. 3: the distribution in the vertical plane is matched to the betatron functions of the ring at the septum, and is shown in Fig. 4. The energy distribution is also uniform within $\pm$1.5%. 1000 particles are tracked for 100 turns taking the injection and extraction septa as aperture limits (-20 mm) in the horizontal plane. The efficiency is still 100%.

Figs. 9÷12 show in the form of histograms the maximum positive and negative amplitudes reached in 100 turns (with the exception of the first one) by the injected particles. The histograms are evaluated at the focusing quadrupole in the arc (where the horizontal β function and the dispersion are near their maximum), in the defocusing one (where the vertical β function is maximum), at the extraction kicker and at the septum in both planes. The same histograms have been calculated for the maximum amplitudes at the first turn between the septum and the kickers, and are presented in Fig. 13 only in the horizontal plane. The negative peak is taken at the focusing sextupole position in the arc, while the positive one is at the end of the second focusing quadrupole downstream the septum position.

3. CLOSED ORBIT CORRECTION

The effective acceptance of the ring can be decreased by closed orbit distortions due to alignment and field errors in magnets. A good orbit correction scheme is necessary to preserve large acceptance as required for injection. The results of the investigation performed on the sensitivity of the previous lattice to different kinds of errors are still valid since the two lattices are very similar [2].

A new layout of monitors and correctors has been studied to better match general layout requirements. The analysis has been performed with the computer code MAD . Several error sets are generated with random distributions; for each one the closed orbit distortion is evaluated at the monitors and corrected. The errors assumed for quadrupoles and bendings are:

magnet misalignments (Δx, Δy)	0.2 mm (rms)
tilts around the horizontal axis ($\Delta\theta$)	0.25 mrad (rms)
tilts around the vertical axis ($\Delta\Phi$)	0.25 mrad (rms)
magnetic field errors ($\Delta B/B$) @ 3 cm	5.0×10^{-4} (rms)

The proposed layout is shown in Fig. 2; it includes 12 monitors (Strip lines + "button" pick-ups, indicated as BPM) and 8 correctors (CHV) acting in both transverse planes. This arrangement might seem redundant in the vertical plane, due to the low betatron tune: however, the large number of monitors and correctors compensates for the lack of available space in the high β regions.

The simulation of the closed orbit correction has been performed in three different cases: with sextupoles off and sextupoles on (with the same errors as in quads) and considering, in addition, monitor alignment errors (Δx, Δy = 0.2 mm).

The results are shown in Tables VI÷VIII : they are averaged over 10 different error sets, before and after correction. Fig. 14 shows the beam positions at the monitors before and after correction in the horizontal plane for one sample without monitor errors; Fig. 15 is the corresponding one for the vertical plane. The uncorrected closed orbit for both transverse planes, as calculated by MAD, is presented in Fig. 16 along the whole lattice.

The results of the simulation show that with the assumed tolerances and without any correction the beam remains within the physical aperture of the ring, thus avoiding the necessity of single turn pick-up systems. The corrected orbits exhibit maximum amplitudes around 1 mm, within the foreseen tolerance for full injection efficiency. The required maximum correction angle is $\alpha_{max} \approx 1.5$ mrad in both planes, leaving some safety margin for localized orbit bumps which might improve injection efficiency during the commissioning of the accumulator.

4. MULTIPOLAR COMPONENTS IN THE MAGNETIC FIELD

The effect of multipolar components in the bending and quadrupole fields has been investigated by checking the stability of large amplitude oscillations with PATRICIA. Due to the quadrupolar component in the bending magnet (field index = 0.5), sextupoles, octupoles and decapoles have been tested as systematic errors.

Table IX gives the fraction of stable trajectories within the physical aperture for multipolar components up to $\Delta B/B = \pm 7.5 \times 10^{-4}$ at 3 cm from the ideal orbit and for energy displacements of the particles within ±1.5%. 12-poles and 20-poles have been considered in the quadrupoles, lower multipoles being negligible if the quadrupolar symmetry is respected: the results are shown in Table X.

From the simulations shown in Tables IX-X it can be concluded that sextupole, octupole and decapole systematic errors below 7.5×10^{-4} at 3 cm from the center of bending magnets can be tolerated if a single multipolar component can account for the total systematic error. In order to give an estimate of the sensitivity to the effect of combined errors with partial compensation, we have studied also the case where the three multipoles add with different signs: Fig. 17 shows the dynamic aperture with a sextupole component $\Delta B/B = -2.5 \times 10^{-4}$, an octupole $\Delta B/B = +2.5 \times 10^{-4}$ and a decapole $\Delta B/B = +2.5 \times 10^{-4}$. Fig. 18 shows the corresponding result with twice the contribution for each multipole. In both cases a small fraction of the trajectories within the physical aperture is unstable.

In the quadrupoles the 12-pole component is not harmful within $\pm 7.5 \times 10^{-4}$ at 3 cm. The 20-pole component seems more dangerous and should be kept below 2.5×10^{-4}, and possibly with the same direction of the quadrupole field.

REFERENCES

[1] M. Zobov, L. Palumbo, private communication.

[2] S. Guiducci, M.R. Masullo, C. Milardi, M.A. Preger: "DAΦNE accumulator update 2", DAΦNE Technical note I-4 (1/10/91).

[3] M.R. Masullo, M. A. Preger: "A new working point for the DAΦNE accumulator", DAΦNE Technical note I-5 (3/12/1991).

TABLE I - MAD output for the linear lattice (1/4 of the ring)

```
                    OTTICA ACCUMULATORE file parameter list

                    ! PHYSICAL ELEMENTS FOLLOW
                5
                    DRIFT,L1,L=1.47943
                    DRIFT,L2,L=0.22
                    DRIFT,L3,L=0.367
                    DRIFT,L4,L=0.208
               10   DRIFT,L5,L=0.440
                    DRIFT,L6,L=0.228
                    DRIFT,L7,L=0.439
                    DRIFT,L8,L=0.349
                    DRIFT,L9,L=0.75
               15   DRIFT,L10,L=0.60043

                    QUAD,QF1,L=0.3,K1=4.70
                    QUAD,QD1,L=0.3,K1=-4.72
                    QUAD,QF2,L=0.3,K1=4.47
               20
                    SBEND,B1,L=.034,ANGLE=0.00773,K1=-0.025845
                    SBEND,B2,L=.034,ANGLE=0.01545,K1=-0.103245
                    SBEND,B3,L=.034,ANGLE=0.02318,K1=-0.232402
                    SBEND,BB,L=0.381,ANGLE=0.346339,K1=-0.413164
               25
                    ! LATTICE STRUCTURE FOLLOWS
                    LINE,HCELL1=(L1,L2,B1,B2,B3,BB,BB,B3,B2,B1,L3,L4,QFT,L5,QD1)

                    LINE,HCELL2=(L6,L6,QF2,L7,B1,B2,B3,BB,BB,B3,B2,B1,L8,L9,L10)
                    LINE,HCELL=(HCELL1,HCELL2)
               30   LINE,PER=(HCELL,-HCELL)
                    LINE,MACC=(2*PER)
```

FINAL VALUES FOR PARAMETERS

PENALTY FCT.	CALL	TIME	E.D.M.	PARAMETER NAME	PAR. VALUE	PAR. ERROR
0.447363E-09	140	0.000	0.719E-09	QF1[K1]	0.471289E+01	0.655920E-05
				QD1[K1]	-0.473852E+01	0.136864E-04
				QF2[K1]	0.449090E+01	0.777706E-05

ELEMENT SEQUENCE				HORIZONTAL						VERTICAL						
POS. NO.	ELEMENT NAME	OCC. NO.	DIST [M]	BETAX [M]	ALFAX	MUX [2PI]	X(CO) [MM]	X'(CO) [MRAD]	DX [M]	DX'	BETAY [M]	ALFAY	MUY [2PI]	Y(CO) [MM]	Y'(CO) [MRAD]	DY [M]	DY'
BEGIN	MACC	1	0.000	2.248	0.000	0.000	0.000	0.000	0.000	0.000	3.979	0.000	0.000	0.000	0.000	0.000	0.000
BEGIN	HCELL	1	0.000	2.248	0.000	0.000	0.000	0.000	0.000	0.000	3.979	0.000	0.000	0.000	0.000	0.000	0.000
BEGIN	HCELL1	1	0.000	2.248	0.000	0.000	0.000	0.000	0.000	0.000	3.979	0.000	0.000	0.000	0.000	0.000	0.000
1	L1	1	1.479	3.222	-0.658	0.093	0.000	0.000	0.000	0.000	4.529	-0.372	0.057	0.000	0.000	0.000	0.000
2	L2	1	1.699	3.533	-0.756	0.103	0.000	0.000	0.000	0.000	4.705	-0.427	0.064	0.000	0.000	0.000	0.000
3	B1	1	1.733	3.585	-0.768	0.105	0.000	0.000	0.000	0.008	4.734	-0.431	0.065	0.000	0.000	0.000	0.000
4	B2	1	1.767	3.637	-0.770	0.106	0.000	0.000	0.001	0.023	4.763	-0.423	0.067	0.000	0.000	0.000	0.000
5	B3	1	1.801	3.689	-0.756	0.108	0.000	0.000	0.002	0.046	4.791	-0.394	0.068	0.000	0.000	0.000	0.000
6	BB	1	2.182	4.086	-0.265	0.123	0.000	0.000	0.085	0.388	4.832	0.289	0.080	0.000	0.000	0.000	0.000
7	BB	2	2.563	4.077	0.288	0.138	0.000	0.000	0.294	0.706	4.368	0.903	0.093	0.000	0.000	0.000	0.000
8	B3	2	2.597	4.057	0.311	0.139	0.000	0.000	0.319	0.726	4.306	0.923	0.094	0.000	0.000	0.000	0.000
9	B2	2	2.631	4.035	0.316	0.140	0.000	0.000	0.344	0.741	4.244	0.923	0.096	0.000	0.000	0.000	0.000
10	B1	2	2.665	4.014	0.310	0.142	0.000	0.000	0.369	0.748	4.181	0.912	0.097	0.000	0.000	0.000	0.000
11	L3	1	3.032	3.823	0.210	0.157	0.000	0.000	0.643	0.748	3.571	0.751	0.112	0.000	0.000	0.000	0.000
12	L4	1	3.240	3.748	0.153	0.165	0.000	0.000	0.799	0.748	3.277	0.660	0.122	0.000	0.000	0.000	0.000
13	QF1	1	3.540	2.324	3.903	0.181	0.000	0.000	0.844	-0.456	4.402	-4.927	0.135	0.000	0.000	0.000	0.000
14	L5	1	3.980	0.242	0.830	0.280	0.000	0.000	0.643	-0.456	9.850	-7.453	0.146	0.000	0.000	0.000	0.000
15	QD1	1	4.280	0.432	-1.550	0.516	0.000	0.000	0.639	0.424	9.965	7.124	0.150	0.000	0.000	0.000	0.000
END	HCELL1	1	4.280	0.432	-1.550	0.516	0.000	0.000	0.639	0.424	9.965	7.124	0.150	0.000	0.000	0.000	0.000
BEGIN	HCELL2	1	4.280	0.432	-1.550	0.516	0.000	0.000	0.639	0.424	9.965	7.124	0.150	0.000	0.000	0.000	0.000
16	L6	1	4.508	1.548	-3.348	0.561	0.000	0.000	0.735	0.424	6.987	5.940	0.155	0.000	0.000	0.000	0.000
17	L6	2	4.736	3.485	-5.145	0.577	0.000	0.000	0.832	0.424	4.548	4.756	0.161	0.000	0.000	0.000	0.000
18	QF2	1	5.036	5.195	0.234	0.588	0.000	0.000	0.788	-0.706	3.494	-0.783	0.174	0.000	0.000	0.000	0.000
19	L7	1	5.475	5.029	0.145	0.601	0.000	0.000	0.478	-0.706	4.271	-0.986	0.192	0.000	0.000	0.000	0.000
20	B1	3	5.509	5.019	0.142	0.602	0.000	0.000	0.454	-0.699	4.338	-0.997	0.193	0.000	0.000	0.000	0.000
21	B2	3	5.543	5.009	0.153	0.603	0.000	0.000	0.431	-0.685	4.406	-0.998	0.195	0.000	0.000	0.000	0.000
22	B3	3	5.577	4.998	0.185	0.605	0.000	0.000	0.408	-0.665	4.473	-0.978	0.196	0.000	0.000	0.000	0.000
23	BB	3	5.958	4.598	0.843	0.617	0.000	0.000	0.211	-0.366	4.988	-0.346	0.209	0.000	0.000	0.000	0.000
24	BB	4	6.339	3.763	1.303	0.632	0.000	0.000	0.132	-0.045	4.980	0.366	0.221	0.000	0.000	0.000	0.000
25	B3	4	6.373	3.674	1.308	0.633	0.000	0.000	0.131	-0.023	4.954	0.398	0.222	0.000	0.000	0.000	0.000
26	B2	4	6.407	3.586	1.295	0.634	0.000	0.000	0.130	-0.008	4.927	0.407	0.223	0.000	0.000	0.000	0.000
27	B1	4	6.441	3.498	1.273	0.636	0.000	0.000	0.130	0.000	4.899	0.403	0.224	0.000	0.000	0.000	0.000
28	L8	1	6.790	2.701	1.012	0.654	0.000	0.000	0.130	0.000	4.647	0.320	0.236	0.000	0.000	0.000	0.000
29	L9	1	7.540	1.605	0.450	0.713	0.000	0.000	0.130	0.000	4.299	0.142	0.262	0.000	0.000	0.000	0.000
30	L10	1	8.141	1.335	0.000	0.780	0.000	0.000	0.130	0.000	4.214	0.000	0.285	0.000	0.000	0.000	0.000
END	HCELL2	1	8.141	1.335	0.000	0.780	0.000	0.000	0.130	0.000	4.214	0.000	0.285	0.000	0.000	0.000	0.000
END	HCELL	1	8.141	1.335	0.000	0.780	0.000	0.000	0.130	0.000	4.214	0.000	0.285	0.000	0.000	0.000	0.000
END	MACC	1	32.563	2.248	0.000	3.120	0.000	0.000	0.000	0.000	3.979	0.000	1.140	0.000	0.000	0.000	0.000

TOTAL LENGTH =	32.563440	QX =	3.119996	QY =	1.140001
		QX' =	-4.398356	QY' =	-4.184695
ALFA =	0.336975E-01	BETAX(MAX) =	5.194891	BETAY(MAX) =	9.965210
GAMMA(TR) =	5.447552	DX(MAX) =	0.844348	DY(MAX) =	0.000000

TABLE II - Parameter list

Energy (GeV)	0.51
Circumference (m)	32.56
Straight section length (m)	3.50
Horizontal betatron wavenumber	3.12
Vertical betatron wavenumber	1.14
Dispersion at Septum Straight Section Center (SSSC) (m)	0.00
Horizontal β at SSSC (m)	2.25
Vertical β at SSSC (m)	3.98
Dispersion at Kicker Straight Section Center (KSSC) (m)	0.13
Horizontal β at KSSC (m)	1.34
Vertical β at KSSC (m)	4.21
Horizontal r.m.s beam size at SSSC (mm, no coupling)	0.75
Vertical r.m.s. beam size at SSSC (mm, full coupling)	1.71
Horizontal r.m.s. beam size at KSSC (mm, no coupling)	0.58
Vertical r.m.s. beam size at KSSC (mm, full coupling)	1.73
Maximum dispersion (m)	0.87
Maximum horizontal β (m)	5.19
Maximum vertical β (m)	11.04
Horizontal betatron damping time (msec)	21.42
Vertical betatron damping time (msec)	21.42
Synchrotron damping time (msec)	10.71
Momentum compaction	0.034
Natural emittance (mm.mrad)	0.253
R.m.s. energy spread (%, radiation only)	0.041
R.m.s. energy spread (%, Z/n=2Ω)	0.091
R.m.s. energy spread (%, Z/n=4Ω)	0.114
Horizontal chromaticity (sextupoles off)	-4.4
Vertical chromaticity (sextupoles off)	-4.2
R.F. frequency (MHz)	73.65
R.F. voltage (KV)	200
Harmonic number	8
Radiated energy per turn (KeV)	5.17
Synchrotron frequency (KHz)	37.76
R.F. energy acceptance (%)	2.98
R.m.s. bunch length (cm, radiation only)	1.75
R.m.s. bunch length (cm, Z/n = 2Ω)	3.85
R.m.s. bunch length (cm, Z/n = 4Ω)	4.86
Beam lifetime (minutes, P=10 ntorr, Z=8, Z/n=0)	33.89

TABLE III - Magnetic strenghts

Bending magnets			
Number	8		
Bending angle (deg)	45		
Bending radius (m)	1.1		
Magnetic length (m)	0.864		
Center field (T)	1.55		
Field index	0.5		
Gradient (T/m)	0.70		
Gap (mm)	42		
Quadrupoles			
Number	12		
Magnetic length (m)	0.3		
Bore radius (mm)	50		
Quadrupole	strength(m^{-2})	gradient(T/m)	pole field (T)
QF1	4.71	8.01	0.401
QD1	4.74	8.06	0.403
QF2	4.49	7.63	0.382
Sextupoles (C_x = C_y =0)			
Number	8		
Magnetic length (m)	0.1		
Bore radius (mm)	50		
Sextupole	strength(m^{-3})	gradient(T/m^2)	pole field (T)
SF	72.9	123.9	0.155
SD	58.7	99.8	0.125

TABLE IV - Injection kicker fields

Integrated field (Gauss	K3	K4	K1	K2
Positrons (sextupoles or	61.1	85.2	85.2	61.1
Electrons (sextupoles on	85.2	61.1	61.1	85.2
Positrons (sextupoles of	60.0	96.1	96.1	60.0
Electrons (sextupoles of	96.1	60.0	60.0	96.1

TABLE V - Extraction kicker fields (both polarities)

X_s (mm)	X'_s(mrad)	Sext.	K3 (G.m)	K4 (G.m)	K1 (G.m)	K2 (G.m)
-28	-1	on	29.7	-80.7	82.1	79.4
-28	1	on	-21.2	-63.7	66.9	64.9
-28	3	on	-57.8	-57.8	59.1	41.2
-28	5	on	-69.7	-56.1	70.6	0.7
-28	-1	off	34.0	-92.6	93.4	93.7
-28	1	off	-3.4	-78.2	80.8	80.4
-28	3	off	-42.5	-66.3	65.6	65.5
-28	5	off	-63.7	-63.7	64.7	35.9

TABLE VI - Closed orbit correction (sextupoles off)
$\Delta x=\Delta y=.2$ mm, $\Delta\Theta=\Delta\Phi=.25$ mrad, $\Delta B/B=5\times10^{-4}$ @ 3 cm

12HV Monitors - 8HV Correctors			
	initial data	**before correction**	**after correction**
X_{rms} (mm)	0	3.65 ± 1.66	.31 ± .17
X_{max} (mm)	0	6.52 ± 2.95	.77 ± .31
Y_{rms} (mm)	0	3.59 ± 1.74	.27 ± .12
Y_{max} (mm)	0	6.89 ± 2.52	.82 ± .43
ηx_{rms} (cm)	54.42	56.4 ± 2.1	54.42 ± .01
ηx_{max} (cm)	84.41	102.2 ± 11.6	84.68 ± .16
ηy_{rms} (cm)	0	10.05 ± 5.04	.36 ± .15
ηy_{max} (cm)	0	17.9 ± 8.3	.69 ± .21
αx_{rms} (mrad)			.50 ± .14
αx_{max} (mrad)			.90 ± .34
αy_{rms} (mrad)			.58 ± .29
αy_{max} (mrad)			1.07 ± .51
Qx	3.12	3.1199 ± .0003	3.1199 ± .0003
Qy	1.14	1.1399 ±. 0005	1.1398 ± .0005
ηx (cm)@ injec.	0	10.6 ± 13.2	.02 ± .40
ηy (cm)@ injec.	0	3.5 ± 9.5	-.2 ± .4

TABLE VII - Closed orbit correction (sextupoles on)
$\Delta x=\Delta y=.2$ mm, $\Delta\Theta=\Delta\Phi=.25$ mrad, $\Delta B/B=5\times10^{-4}$ @ 3 cm

12HV Monitors - 8HV Correctors			
	initial data	**before correction**	**after correction**
X_{rms} (mm)	0	3.63 ± 1.66	.31 ± .16
X_{max} (mm)	0	6.54 ± 2.95	.77 ± .31
Y_{rms} (mm)	0	3.63 ± 1.62	.27 ± .12
Y_{max} (mm)	0	6.86 ± 2.46	.82 ± .43
ηx_{rms} (cm)	54.42	54.61 ± .16	54.42 ± .03
ηx_{max} (cm)	84.41	90.33 ± 2.67	85.37 ± .79
ηy_{rms} (cm)	0	4.92 ± 2.04	1.26 ± .63
ηy_{max} (cm)	0	9.37 ± 3.28	1.99 ± 1.04
αx_{rms} (mrad)			.50 ± .13
αx_{max} (mrad)			.90 ± .34
αy_{rms} (mrad)			.58 ± .29
αy_{max} (mrad)			1.07 ± .51
Qx	3.12	3.119 ± .004	3.120 ± .002
Qy	1.14	1.140 ± .001	1.139 ± .002
ηx (cm)@ injec.	0	2.39 ± 2.46	.1 ± .8
ηy (cm)@ injec.	0	1.32 ± 4.62	-.34 ± 1.45

TABLE VIII - Closed orbit correction (sextupoles on)
$\Delta x=\Delta y=$ 0.2 mm, $\Delta\Theta,\Delta\Phi$=0.25 mrad, $\Delta B/B=5x10^{-4}$ @ 3 cm
Monitor alignment error $\Delta x=\Delta y$=0.2 mm

12HV Monitors - 8HV Correctors			
	initial data	**before correction**	**after correction**
X_{rms} (mm)	0	3.63 ± 1.66	.35 ± .08
X_{max} (mm)	0	6.54 ± 2.95	.85 ± .22
Y_{rms} (mm)	0	3.63 ± 1.62	.32 ± .08
Y_{max} (mm)	0	6.86 ± 2.46	.88 ± .33
ηx_{rms} (cm)	54.42	54.61 ± .16	54.43 ± .03
ηx_{max} (cm)	84.41	90.33 ± 2.67	85.40 ± .82
ηy_{rms} (cm)	0	4.92 ± 2.04	1.11 ± .45
ηy_{max} (cm)	0	9.37 ± 3.28	2.10 ± 1.07
αx_{rms} (mrad)			.49 ± .13
αx_{max} (mrad)			.88 ± .19
αy_{rms} (mrad)			.59 ± .24
αy_{max} (mrad)			1.08 ±. 45
Qx	3.12	3.119 ± .004	3.120 ± .002
Qy	1.14	1.140 ± .001	1.139 ± .002
ηx (cm)@ injec.	0	2.39 ± 2.46	-.06 ± .91
ηy (cm)@ injec.	0	1.32 ± 4.62	-.3 ± 1.3

TABLE IX - Multipolar components in bending magnets

Sextupole in bendings

$\Delta B/B$@ 3cm	-7.5×10^{-4}	-5×10^{-4}	5×10^{-4}	7.5×10^{-4}
	stable trajectories (%) inside physical a [34x28 mm^2]			
$\Delta E/E$=-1.5%	100	100	100	100
$\Delta E/E$= 0	100	100	100	100
$\Delta E/E$=+1.5%	100	100	100	100

Octupole in bendings

$\Delta B/B$@ 3 cm	-7.5×10^{-4}	-5×10^{-4}	5×10^{-4}	7.5×10^{-4}
	stable trajectories (%) inside physical a [34x28mm^2]			
$\Delta E/E$=-1.5%	97.5	100	100	100
$\Delta E/E$= 0	100	100	100	100
$\Delta E/E$= 1.5%	100	100	100	100

decapole in bendings

$\Delta B/B$@ 3 cm	-7.5×10^{-4}	-5×10^{-4}	5×10^{-4}	7.5×10^{-4}
	stable trajectories (%) inside physical a [34x28 mm^2]			
$\Delta E/E$=-1.5%	100	100	100	100
$\Delta E/E$ = 0	100	100	100	100
$\Delta E/E$= 1.5%	100	100	100	100

TABLE X - Multipolar components in quadrupoles

12-pole in quads

$\Delta B/B$@ 3 cm	-7.5×10^{-4}	-5×10^{-4}	5×10^{-4}	7.5×10^{-4}
	stable trajectories (%) inside physical a [34x28 mm^2]			
$\Delta E/E$=-1.5%	100	100	100	100
$\Delta E/E$=0%	100	100	100	100
$\Delta E/E$=+1.5%	100	100	100	100

20-pole in quads

$\Delta B/B$@ 3 cm	-5×10^{-4}	-2.5×10^{-4}	2.5×10^{-4}	5×10^{-4}
	stable trajectories (%) inside physical a [34x28 mm^2]			
$\Delta E/E$=-1.5%	85	95	97.5	95
$\Delta E/E$=0%	100	100	100	100
$\Delta E/E$=+1.5%	100	100	100	100

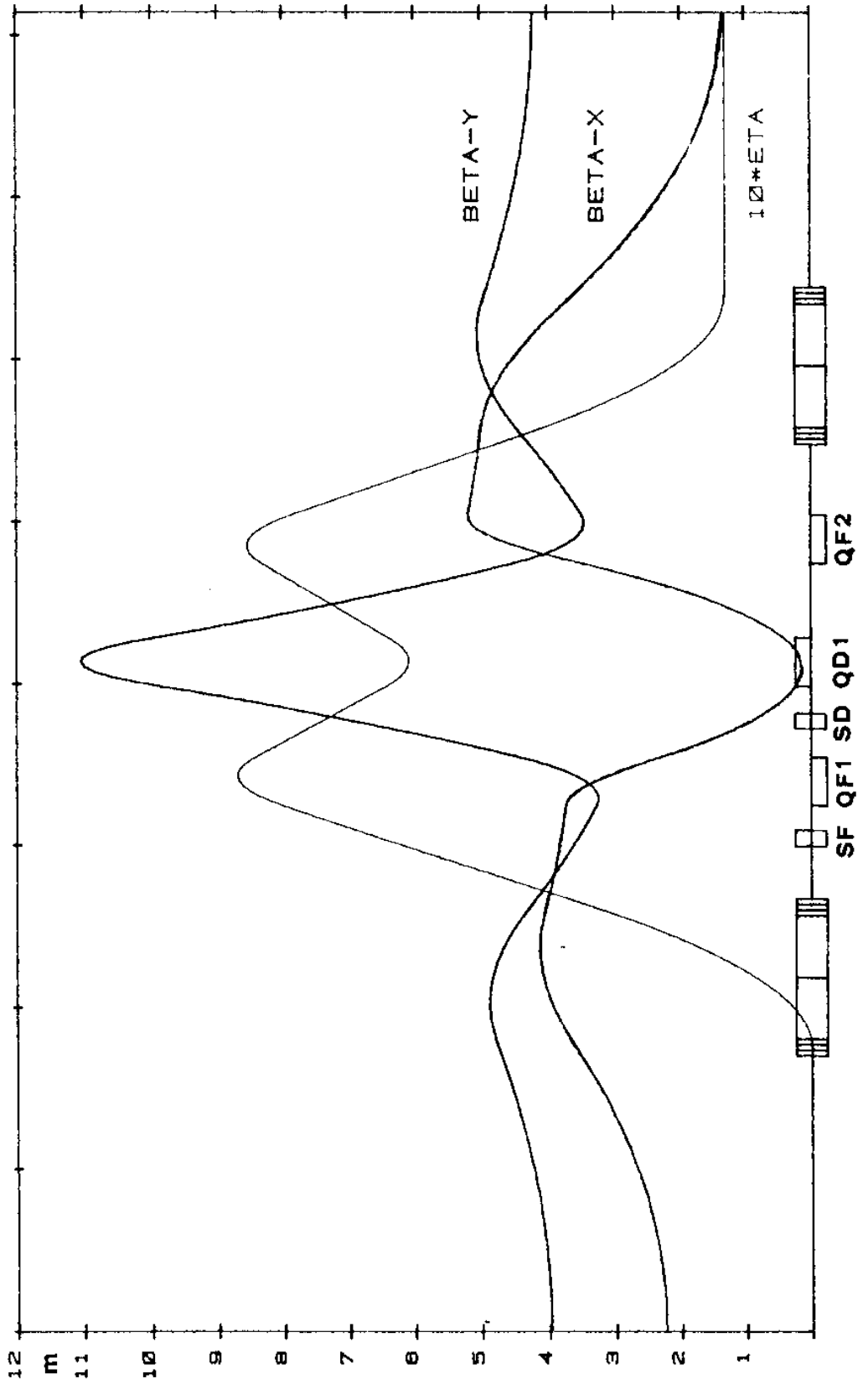

Figure 1 - Optical functions for 1/4 of the ring

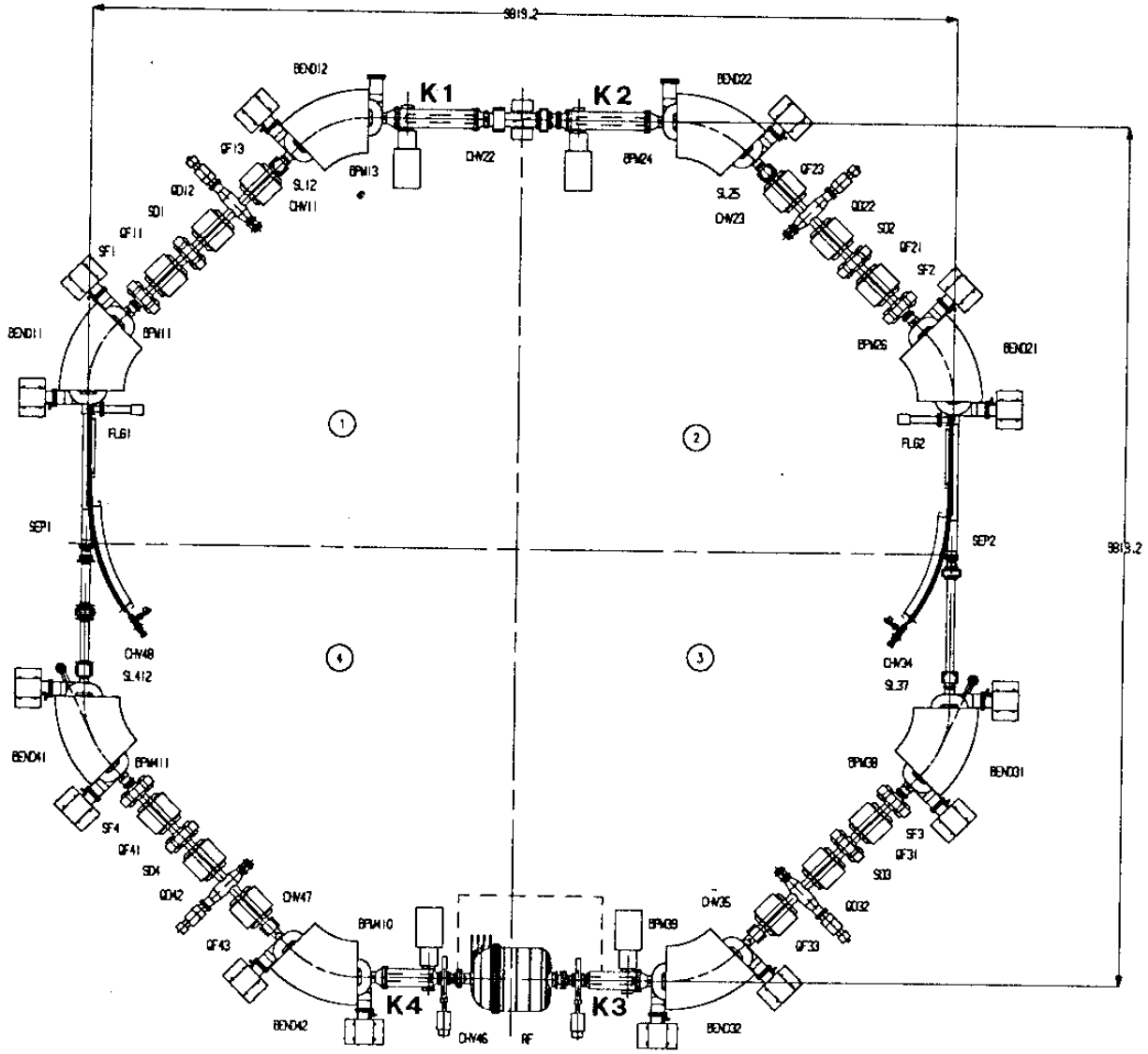

Figure 2 - Accumulator layout

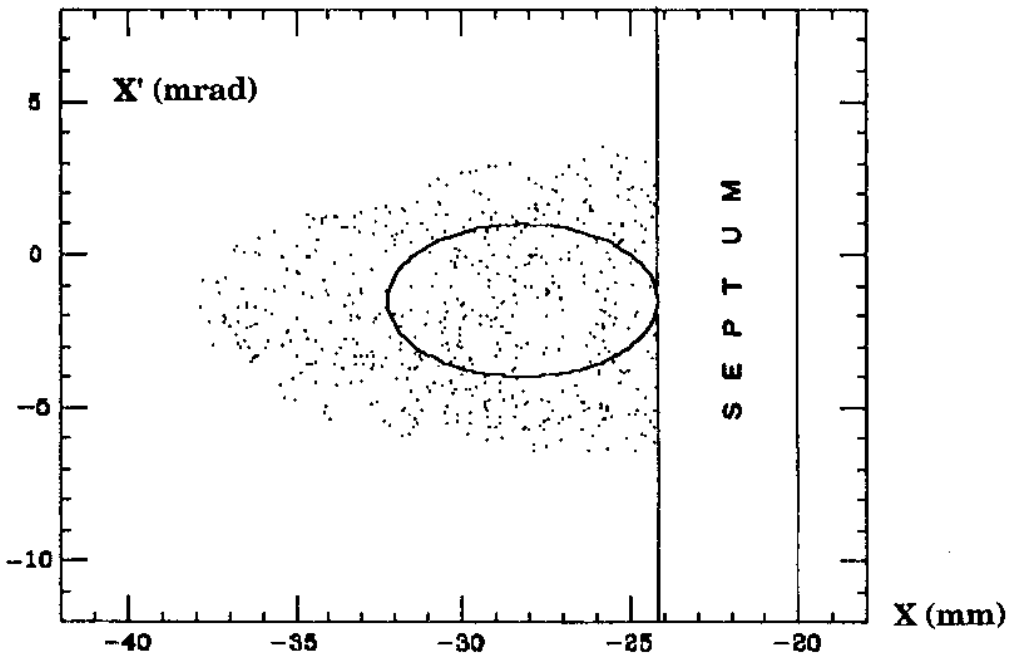

Figure 3 - **Accumulator acceptance in the horizontal betatron space at the septum. The ellipse represents the incoming beam with ε = 10 mm mrad, β = 1.6 m, α = 0**

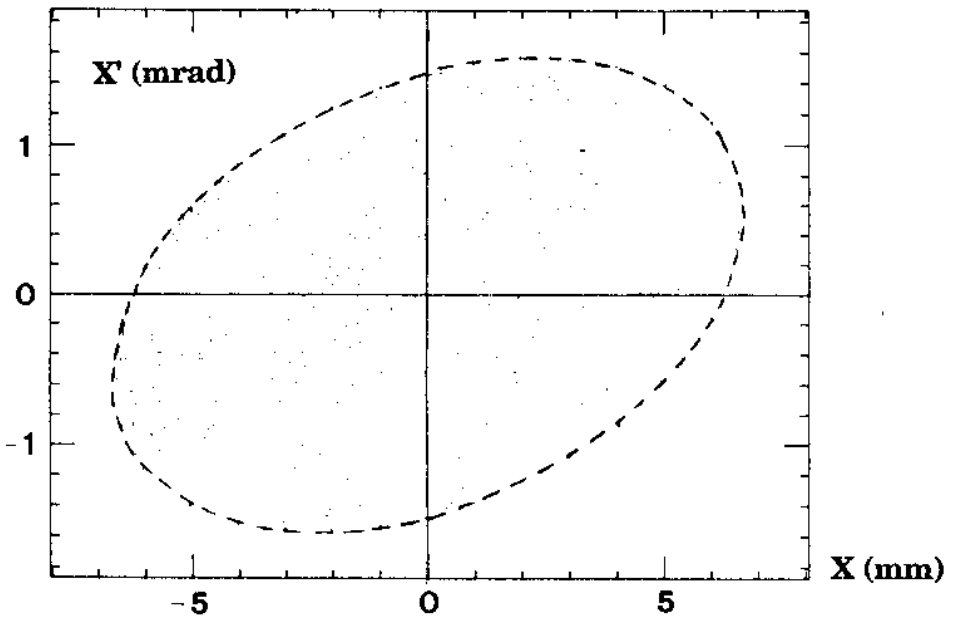

Figure 4 - **Phase space distribution of tracked particles in the vertical plane with ε = 10 mm·mrad, β = 4.53 m, α = -0.37**

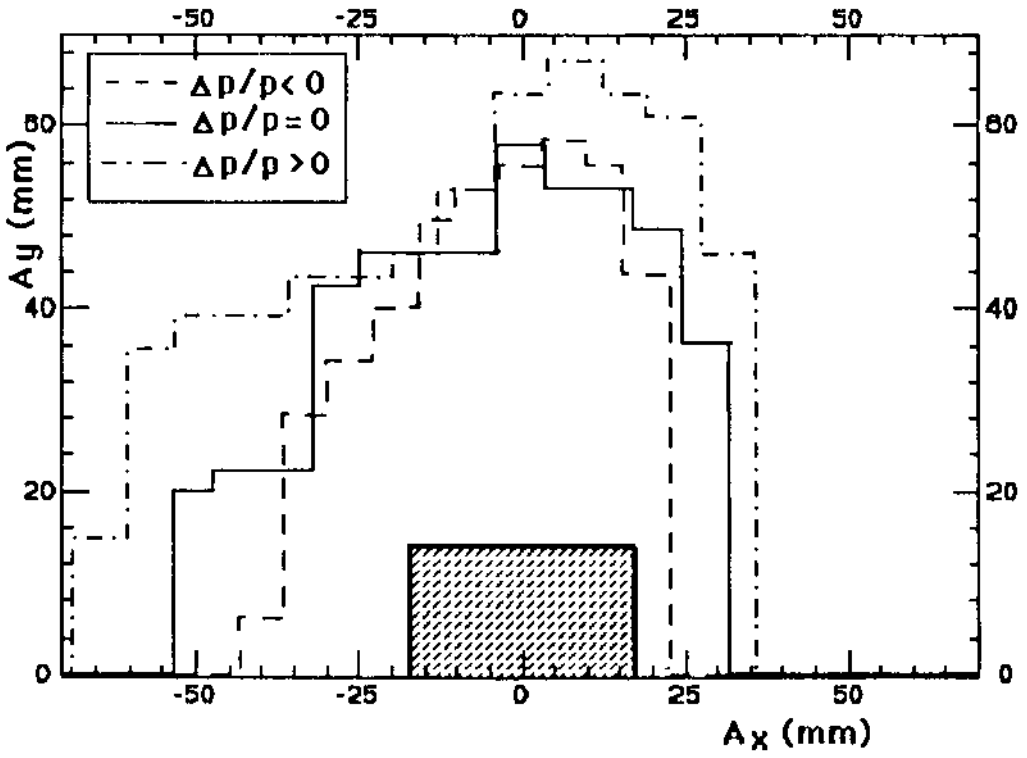

Figure 5 - Dynamic aperture for the ideal machine. ΔE/E = 0, +1.5%, -1.5% with sextupoles at the nominal working point with $C_x = C_y = 0$

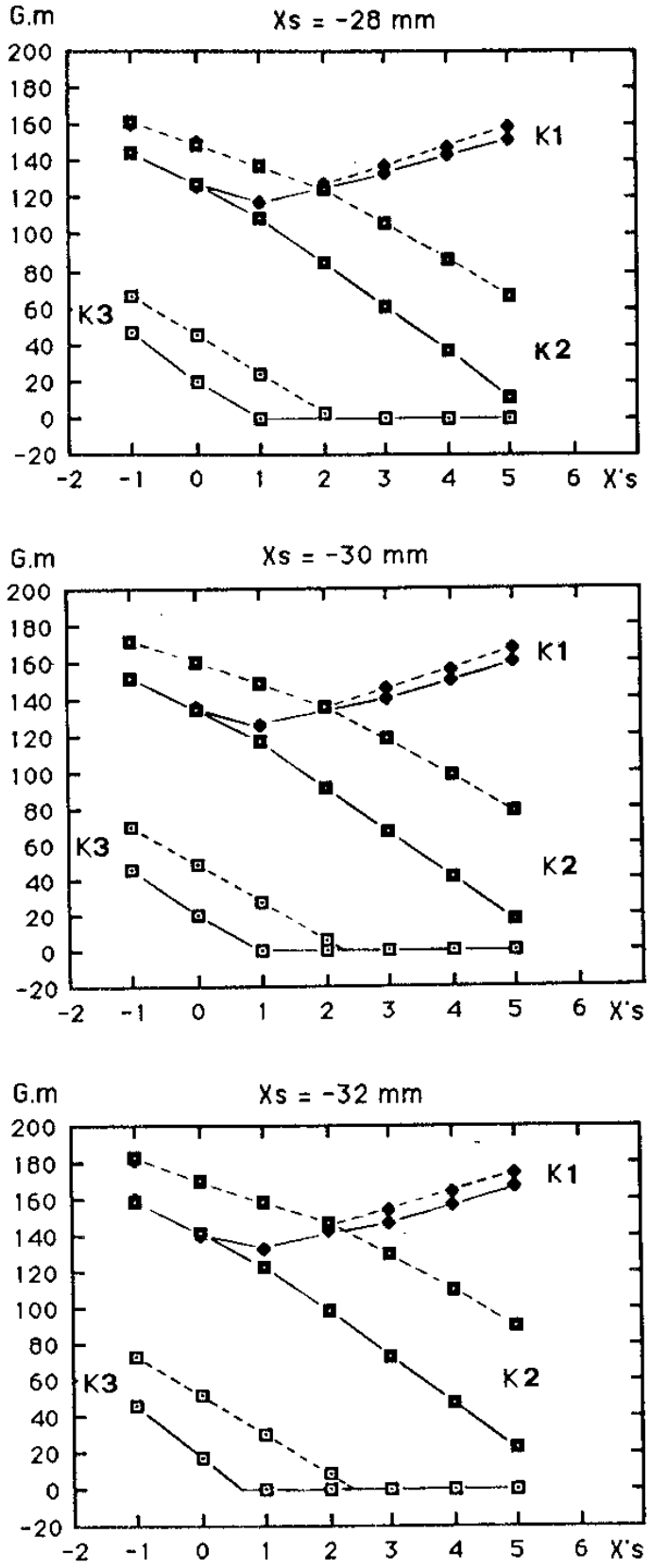

Figure 6 - Integrated field in the kickers at extraction as a function of extraction angle.

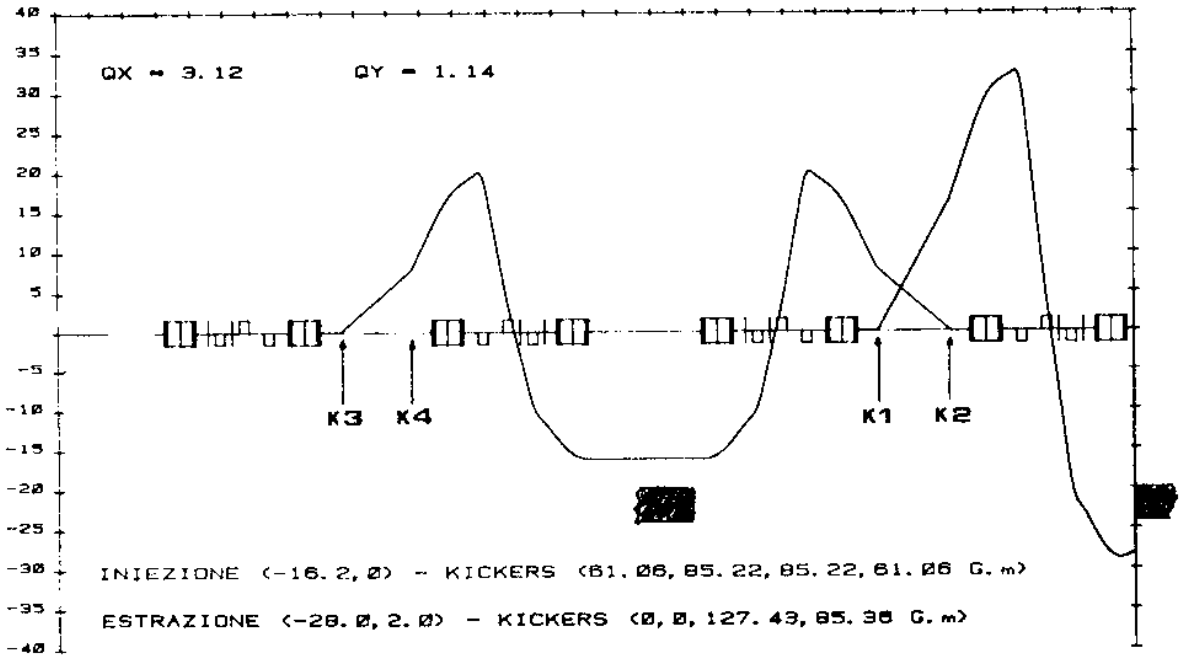

Figure 7 - Injection and extraction trajectories with positive polarity in all kickers.

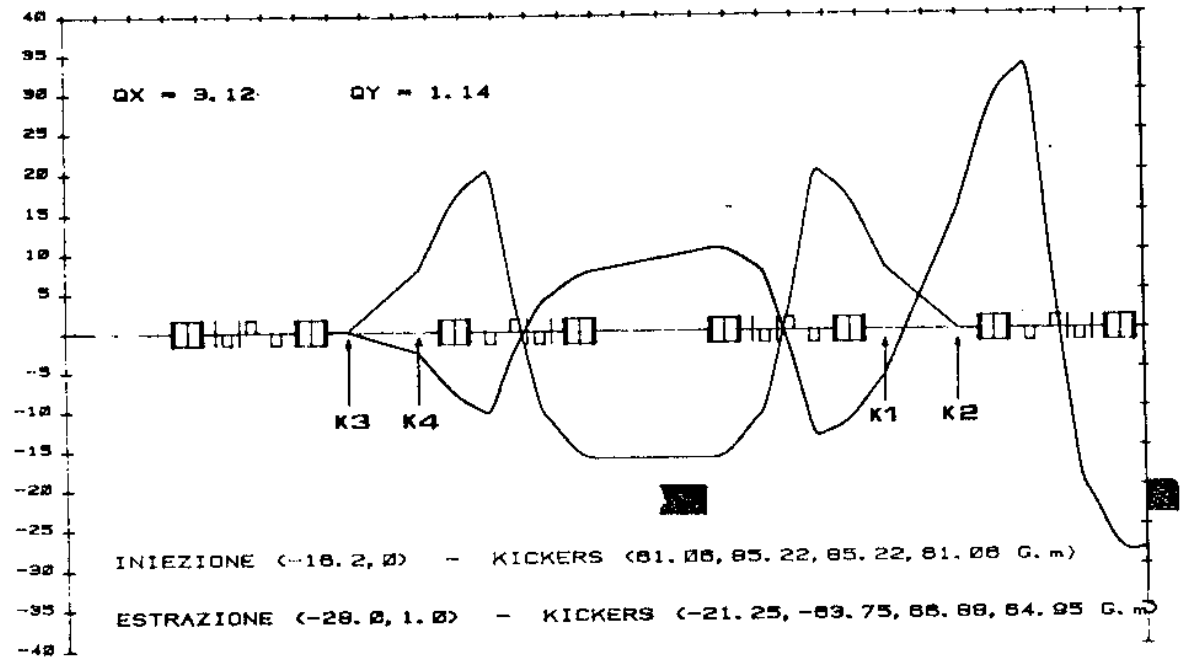

Figure 8 - Injection and extraction trajectories with both polarities in the kickers.

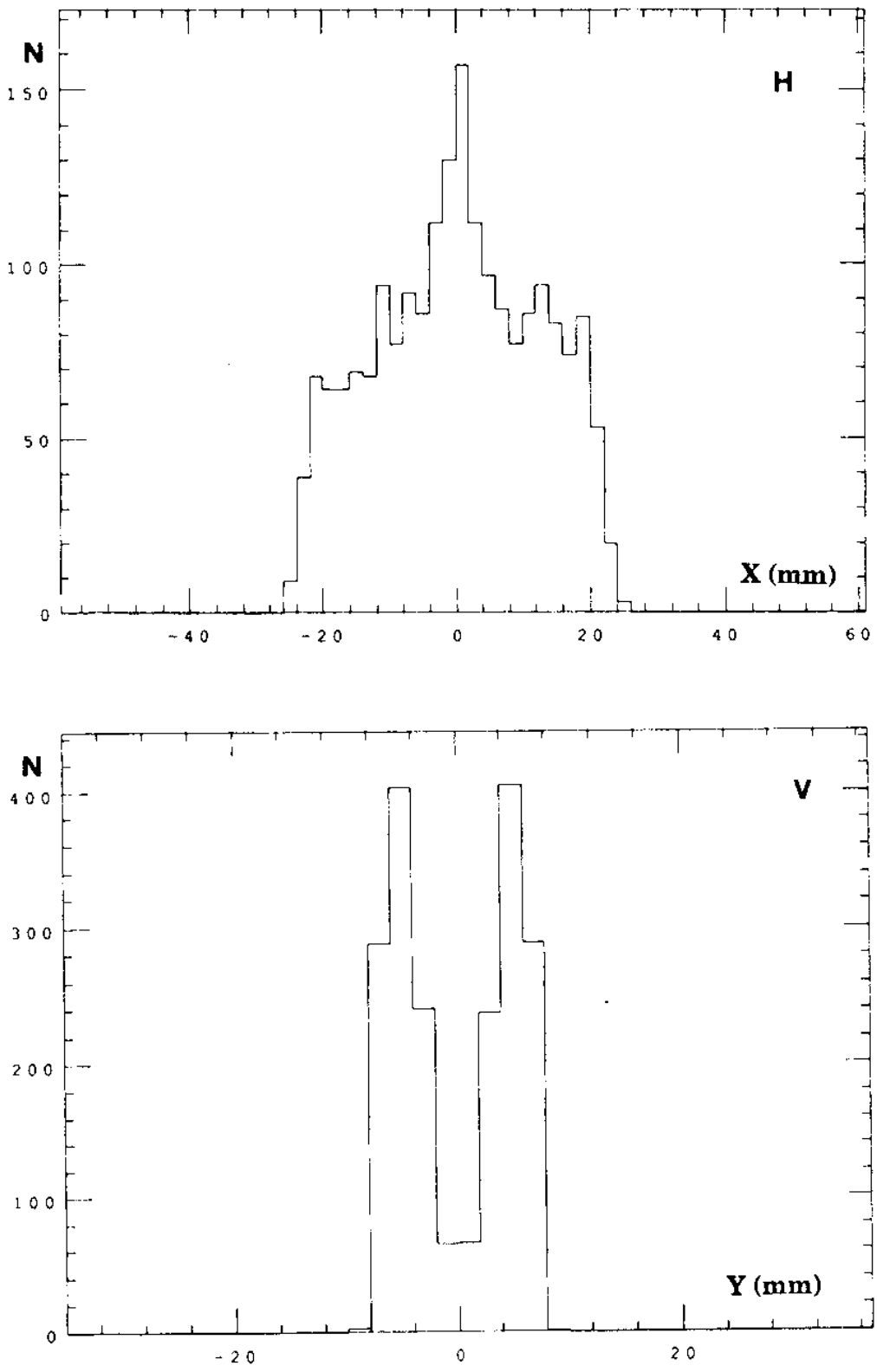

Figure 9 - Horizontal and vertical maximum amplitudes of the tracked particles in the first focusing quadrupole in the arc (QF1) during the first 100 revolutions

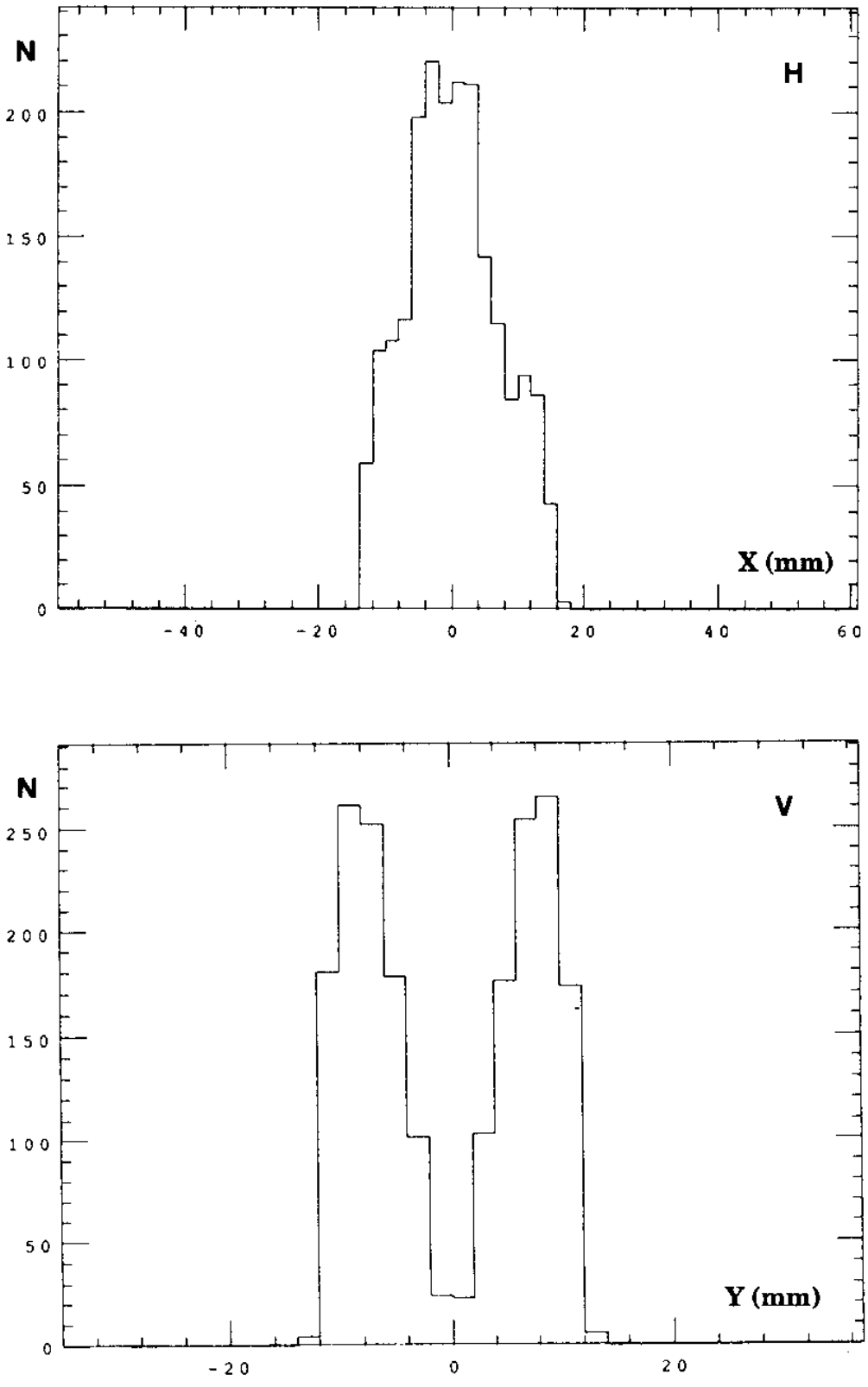

Figure 10 - Horizontal and vertical maximum amplitudes of the tracked particles in the defocusing quadrupole in the arc (QD1) during the first 100 revolutions

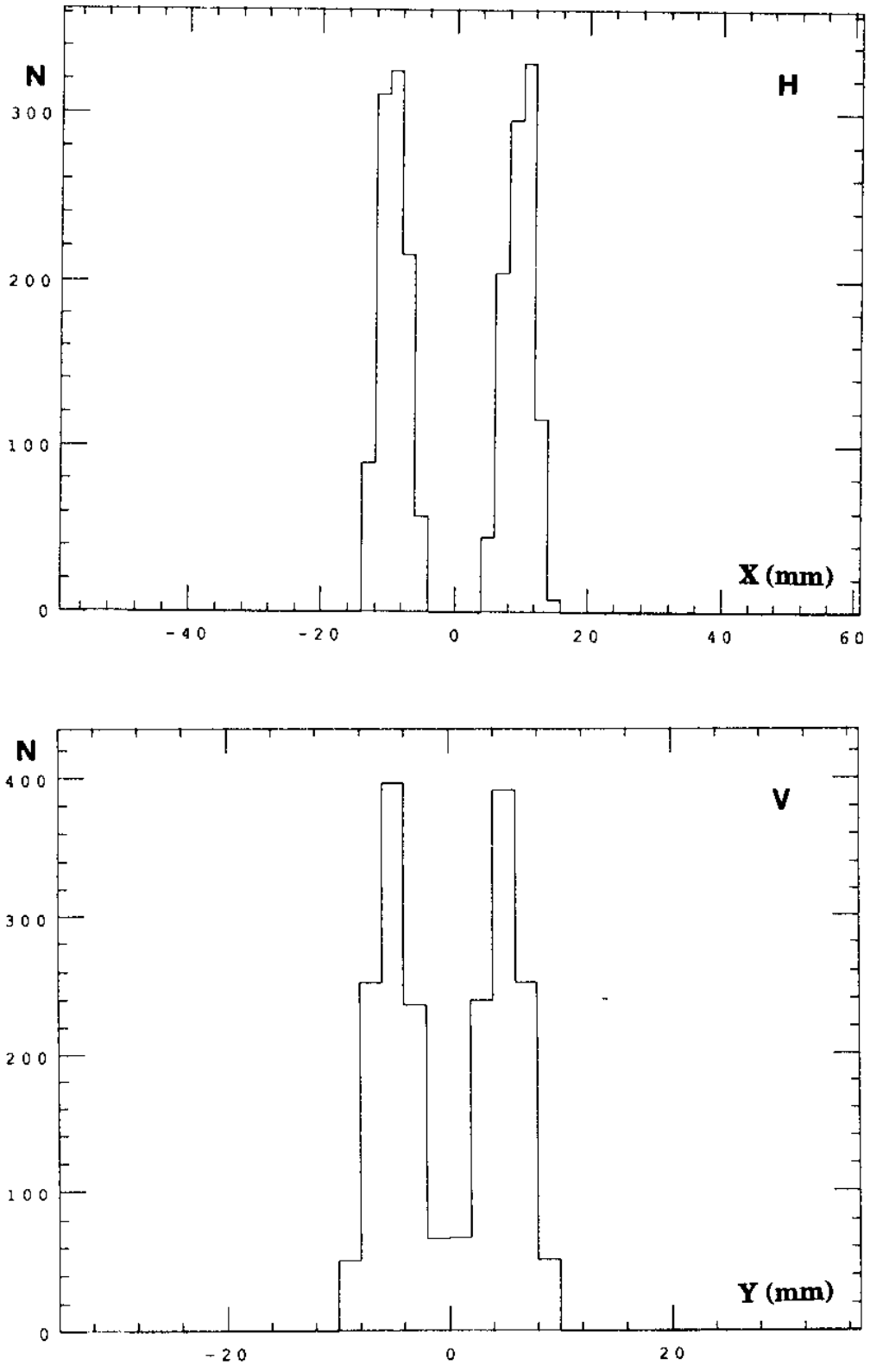

Figure 11 - Horizontal and vertical maximum amplitudes of the tracked particles in the kickers during the first 100 revolutions

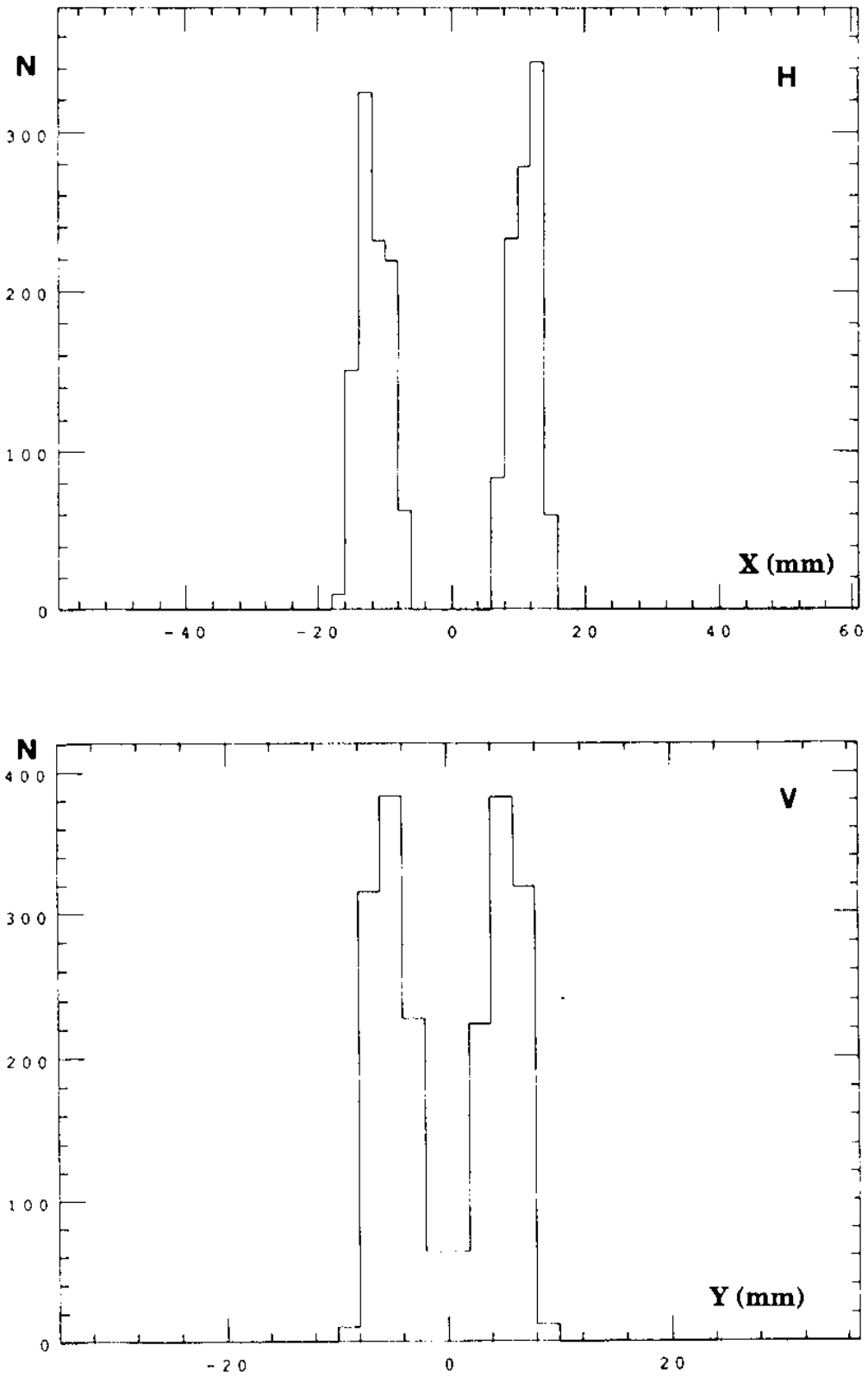

Figure 12 - Horizontal and vertical maximum amplitudes of the tracked particles at the septum during the first 100 revolutions

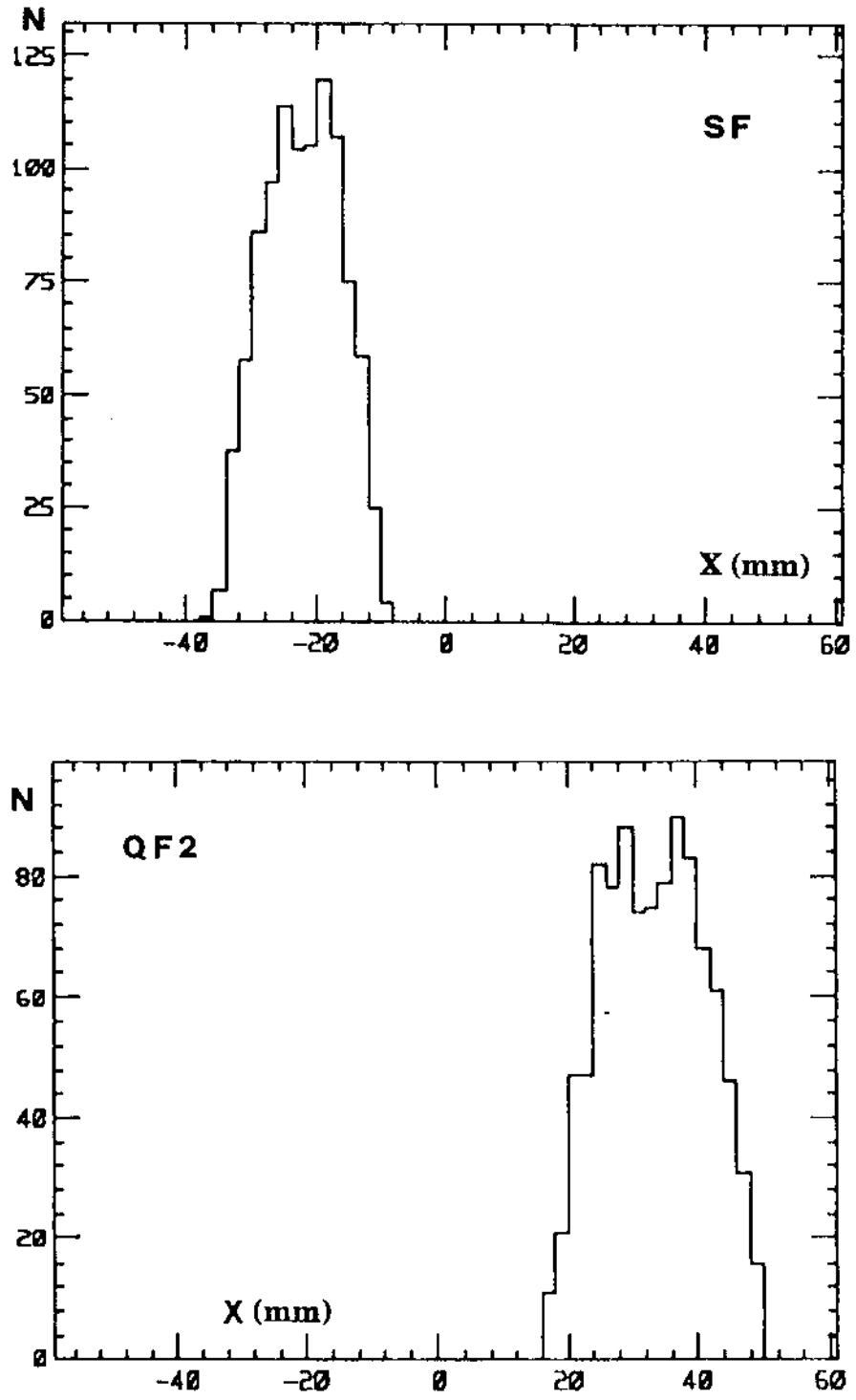

Figure 13 - Horizontal amplitudes of the tracked particles in the first turn in the focusing sextupole (SF) and second focusing quadrupole (QF2) downstream the injection septum.

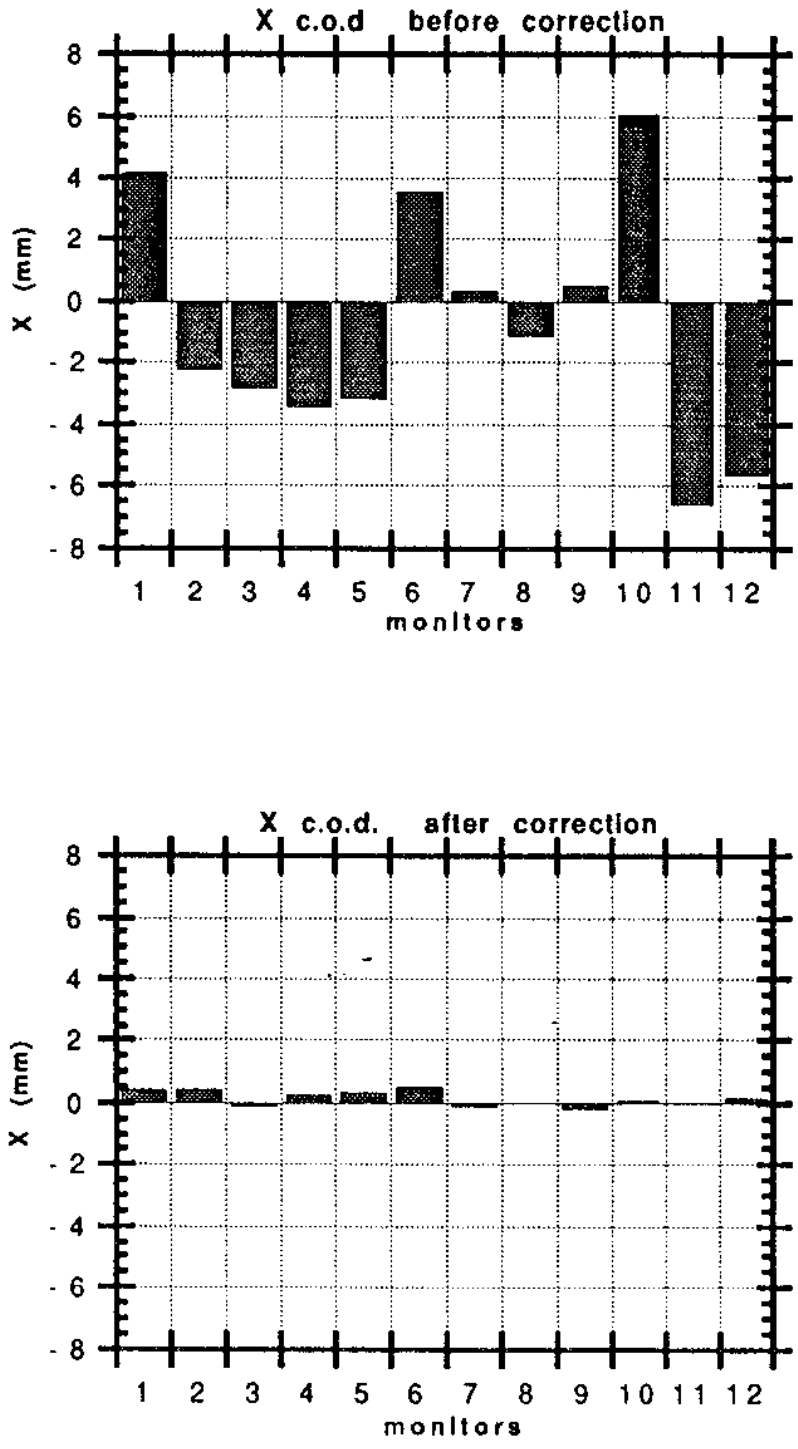

Figure 14 - Sample closed orbit with alignment and field errors at the monitors before and after correction in the horizontal plane

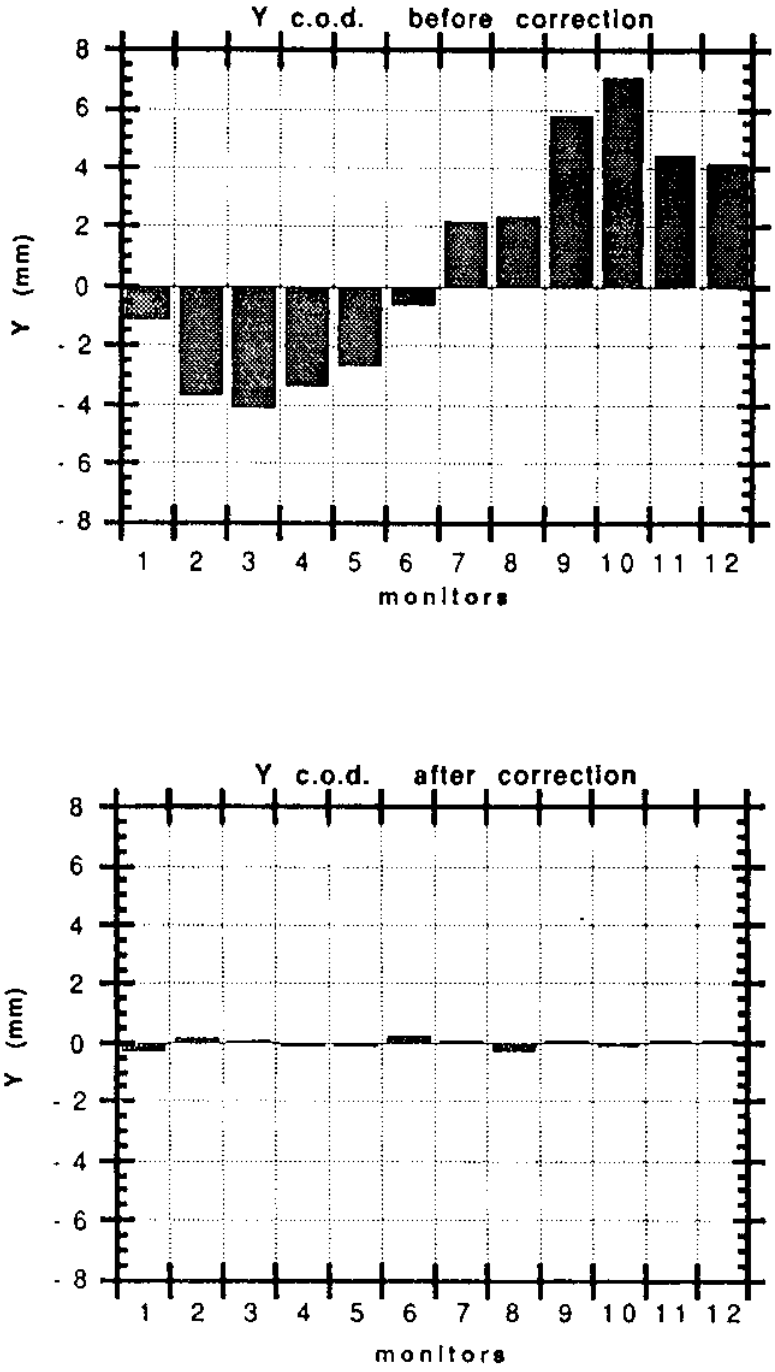

Figure 15 - Sample closed orbit with alignment and field errors at the monitors before and after correction in the vertical plane

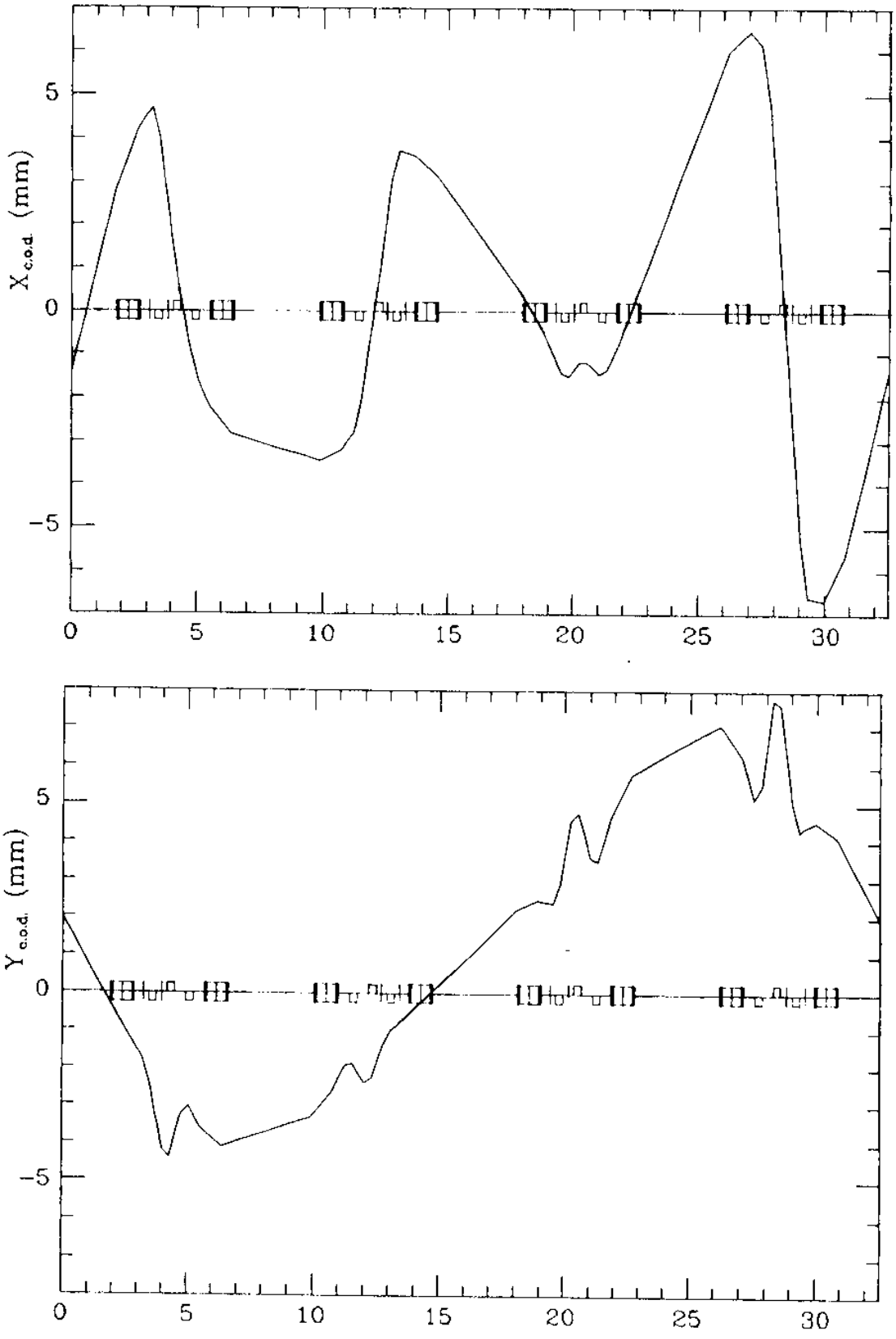

Figure 16 - Sample close orbit with alignment and field errors in the whole ring in the horizontal (high) and vertical (low) planes

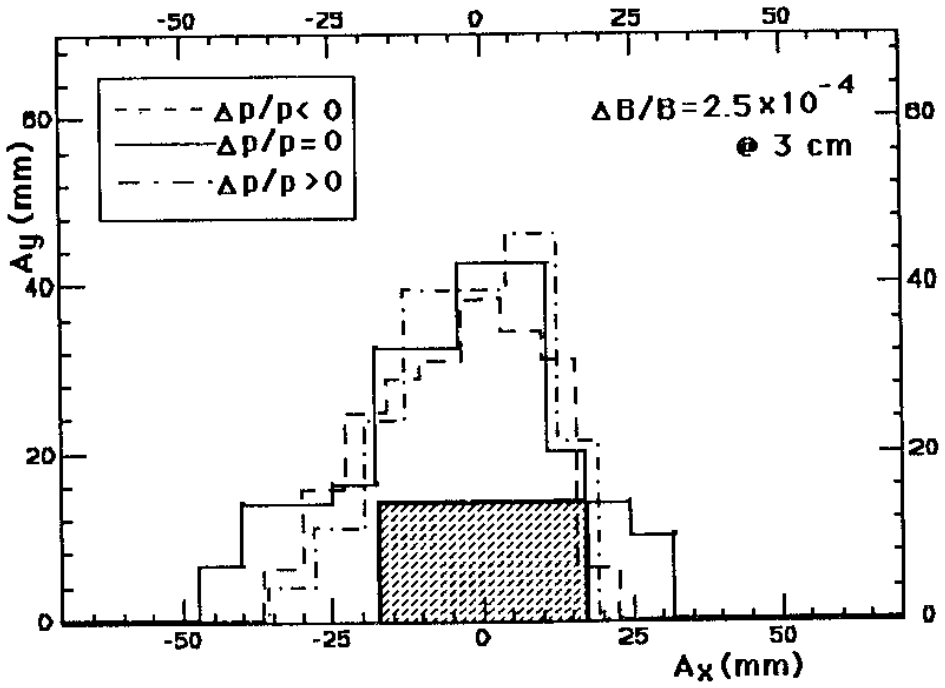

Figure 17 - Dynamic aperture with multipolar components in the bending magnet field (sextupole = -2.5×10^{-4}, octupole = $+2.5\times10^{-4}$, decapole = $+2.5\times10^{-4}$ at 3 cm from the center)

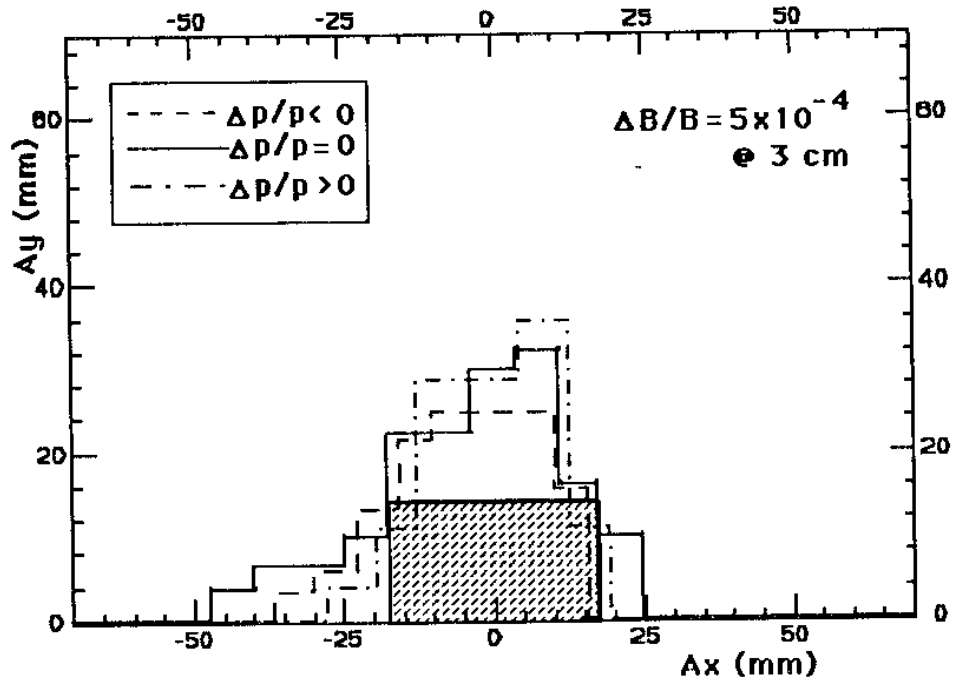

Figure 18 - Dynamic aperture with multipolar components in the bending magnet field (sextupole = -5×10^{-4}, octupole = $+5\times10^{-4}$, decapole = $+5\times10^{-4}$ at 3 cm from the center)